McCray *et al. Acta Neuropathologica Communications* (2024) 12:154
https://doi.org/10.1186/s40478-024-01855-3

Acta Neuropathologica Communications

RESEARCH Open Access

Trem2-deficiency aggravates and accelerates age-related myelin degeneration

Tyler J. McCray[1], Logan M. Bedford[1], Stephanie J. Bissel[1,2†] and Bruce T. Lamb[1,2*†]

Abstract
Aging is the greatest known risk factor for most neurodegenerative diseases. Myelin degeneration is an early pathological indicator of these diseases and a normal part of aging; albeit, to a lesser extent. Despite this, little is known about the contribution of age-related myelin degeneration on neurodegenerative disease. Microglia participate in modulating white matter events from demyelination to remyelination, including regulation of (de) myelination by the microglial innate immune receptor triggering receptor expressed on myeloid cells 2 (TREM2). Here, we demonstrate Trem2-deficiency aggravates and accelerates age-related myelin degeneration in the striatum. We show TREM2 is necessary for remyelination by recruiting reparative glia and mediating signaling that promotes OPC differentiation/maturation. In response to demyelination, TREM2 is required for phagocytosis of large volumes of myelin debris. In addition to lysosomal regulation, we show TREM2 can modify the ER stress response, even prior to overt myelin debris, that prevents lipid accumulation and microglial dysfunction. These data support a role for Trem2-dependent interactions in age-related myelin degeneration and suggest a basis for how early dysfunctional microglia could contribute to disease pathology through insufficent repair, defective phagocytosis, and the ER stress response.

Keywords Microglia, Aging, TREM2, White matter, Myelin degeneration, Neurodegeneration

Introduction

Aging is the greatest known risk factor for various dementias and neurodegenerative diseases including Alzheimer's disease (AD). Although pathological hallmarks of AD invariably include extracellular beta-amyloid (Aβ) plaques, neurofibrillary tangles, and glial activation, proteomic studies and genetic network analyses have recently highlighted changes in myelination, oligodendrocytes, and neurofilaments as players in AD [43, 68]. White matter degeneration has been shown to be an early clinical and pathological marker of AD and may even precede Aβ plaques [18, 38]. Further, white matter tracts have been identified as vulnerable foci during aging [12, 13, 26]. Despite this, the molecular mechanisms of white matter degeneration have been a drastically understudied component of both aging and AD pathogenesis.

Myelin volume reaches a maximal at around age 45–50 and then begins a steady decline until death [67]. This reduction in myelin volume can coincide with the emergence of pronounced AD pathology. Myelin degeneration has been implicated in contributing to and exacerbating amyloid deposition, tau aggregation, chronic neuroinflammation, and axonal damage [17, 18, 56]. Over the last decade, an abundance of evidence points toward the immune response and inflammation as integral

†Stephanie J. Bissel and Bruce T. Lamb contributed equally to this work.

*Correspondence:
Bruce T. Lamb
btlamb@iu.edu
[1]Stark Neurosciences Research Institute, Indiana University, School of Medicine, Indianapolis IN 46202, USA
[2]Department of Medical and Molecular Genetics, Indiana University, School of Medicine, Indianapolis IN 46202, USA

© The Author(s) 2024. **Open Access** This article is licensed under a Creative Commons Attribution-NonCommercial-NoDerivatives 4.0 International License, which permits any non-commercial use, sharing, distribution and reproduction in any medium or format, as long as you give appropriate credit to the original author(s) and the source, provide a link to the Creative Commons licence, and indicate if you modified the licensed material. You do not have permission under this licence to share adapted material derived from this article or parts of it. The images or other third party material in this article are included in the article's Creative Commons licence, unless indicated otherwise in a credit line to the material. If material is not included in the article's Creative Commons licence and your intended use is not permitted by statutory regulation or exceeds the permitted use, you will need to obtain permission directly from the copyright holder. To view a copy of this licence, visit http://creativecommons.org/licenses/by-nc-nd/4.0/.

contributors to AD pathology and age-related myelin degeneration, implicating microglia as critical modulators of disease progression.

In the healthy adult CNS, microglia, amongst other glia, serve to maintain and support white matter via three broad events: demyelination, oligodendrogenesis, and remyelination [34, 41]. Their ability to respond to and engage myelin damage is crucial for proper debris clearance during demyelination [9, 36]. Along with astrocytes, microglia participate in the complex interplay of inflammatory and anti-inflammatory signaling during oligodendrogenesis [19, 34, 41]. They release chemokines such as CXCL1, IL-1β, and CXCL12 to recruit oligodendrocyte precursor cells (OPCs) to areas of demyelination, cytokines like TNF-α and IL-6 to support OPC proliferation, and trophic factors such as brain-derived neurotrophic factor (BDNF), insulin growth factor 1 (IGF-1), and galectin-3 (gal-3) to promote differentiation of OPCs into mature myelinating oligodendrocytes [15, 29, 46, 51]. Failure of any of these steps leads to unresolved damage and lack of subsequent remyelination.

Aging can exert a pronounced impact on glia and their functions. In the diseased or aging CNS, there are a host of morphological, transcriptomic, and functional changes to glial populations. Microglia and astrocytes display a diminished ability to respond to damage, impaired phagocytosis and debris clearance, reduced trophic support, and increased aberrant activation and inflammation [7, 25]. Oligodendrocytes are exceedingly susceptible to this inflammation and oxidative stress, resulting in a reduction in their regenerative capacity and remyelination efficiency [14, 16, 61]. Importantly, evidence suggests that microglia considerably regulate the other two glial populations [41, 44, 51]. These microglial phenotypic changes are highly dynamic and heterogenous and are dependent on brain region, pathology, and age [25, 30, 69]. Identification of microglial subtypes such as white matter-associated microglia (WAM) and disease-associated microglia (DAM) has implicated the innate immune receptor Triggering Receptor Expressed on Myeloid Cells 2 (TREM2) as a crucial modulator of these transition states in both aging and disease [33, 57].

In the brain, TREM2 is located predominantly on microglia and is highly expressed in white-matter regions [22]. TREM2 activity is linked to a variety of diseases that display white matter-pathology such as Nasu-Hakola disease (NHD), frontotemporal lobar degeneration (FTLD), and multiple sclerosis (MS) [3, 10, 37, 50]. Further, TREM2 is necessary for damage-associated lipid sensing that initiates a cascade of microglial responses to myelin damage [48, 64]. These responses include microglial activation, migration, and expansion at sites of demyelination followed by subsequent phagocytosis and lipid metabolism [8, 10, 48, 52]. In addition, TREM2 expression increases with age, making it of particular interest to investigate how it influences age-related myelin degeneration [22].

Recent white matter studies investigating TREM2 have largely focused on the changes to microglia in response to induced demyelination. There has been less emphasis on how TREM2 may impact and contribute to progression of age-related demyelination. Moreover, a large portion of these studies utilize various chemical modifiers (e.g., lysolecithin, cuprizone, etc.) to initiate exacerbated demyelinating phenotypes that may not entirely reflect typical demyelination. The regions analyzed in these studies have also been relatively limited to white matter present in the hippocampus, cortex, and corpus callosum. Given the impact of region and age on the functional heterogeneity of both microglia and TREM2, it remains important to consider the results in other contexts to determine if they are broadly applicable. While these studies provide useful insight, these limitations make these studies difficult to interpret cohesively. Thus, it is important to elucidate which white-matter outcomes are a consequence of age, region, TREM2, and additive effects of these variables.

Here, we use aged wild-type C57BL/6J (WT) and Trem2-knockout ($Trem2^{-/-}$) mice to assess the effect of TREM2 on white matter degeneration, glial populations, and signaling. Due to its increased age-related vulnerability, disease relevance, and importance as a signaling hub, the striatum was selected as an important region of interest [12, 13, 26, 69]. Further, we use primary microglial cells from WT and $Trem2^{-/-}$ mice to assess myelin phagocytosis and dissect the mechanisms by which TREM2 impacts the microglial response. In this study, we aim to answer the following questions: (1) how TREM2 modifies age-related myelin degeneration; (2) which cell types are affected; (3) what aspects in the response TREM2 mediates?

Materials and methods

Models

Wild-type C57BL/6J (B6; referred to as WT in text) (Stock #: 000664) and $Trem2^{-/-}$ (Stock #: 027197) mice were obtained from Jackson Laboratory. Male and female mice aged postnatal day 3–5 for were utilized for in vitro experiments, while mice aged 6, 12, and 18 months were used for in vivo experiments. Mice were housed with up to five mice per cage and fed a 9% fat diet (Teklad Global, 2019 S) throughout the aging process.

Mice were housed in Indiana University School of Medicine (IUSM) animal facilities, which are accredited by the Association and Accreditation of Laboratory Animal Care. Animals were maintained according to the National Institutes of Health Guide for the Care and Use

of Laboratory Animals. Experiments were approved by the IUSM Institutional Animal Care and Use Committee.

Tissue processing

Mice were anesthetized with ketamine/xylazine and perfused with ice-cold PBS between 11AM-1PM to minimize circadian effects. Brains were removed and separated into two hemispheres to be used for immunohistochemistry and protein or RNA analyses.

The hemispheres to be used for immunohistochemistry were drop-fixed in 4% PFA for 24–48 h at 4˚C, then transferred and stored in 30% sucrose in PBS at 4˚C until the brains sunk. Brains were embedded in O.C.T compound (Tissue-Tek, 4583) and cryosectioned into 30-µm free-floating sections. Sections were stored in 0.05% sodium azide in PBS at 4˚C until use.

The hemispheres used for protein analyses were microdissected into cortical and white-matter containing regions (striatum, corpus callosum, cerebellum/brainstem). Brain tissues were snap frozen in liquid nitrogen and stored at -80˚C until use. Frozen microdissected-regions were homogenized in ice-cold T-PER Tissue Protein Extraction Reagent (Thermo Fisher, 78510) supplemented with phosphatase inhibitor cocktail (1:100, Sigma, P5726) and protease inhibitor cocktail (1:100, Sigma, P8340) at a 1 mg:10mL tissue weight to reagent volume. Homogenization was carried out on ice using a PowerGen 125 homogenizer (Fisher) at 75% of max speed for 1 min followed by sonication using a SLPe Digital Sonifier (Branson) at a continuous 30% amplitude for 10 s. Homogenized white-matter samples were spun down at 15,000 rpm using an Eppendorf 5424R centrifuge at 4˚C for 30 min, then supernatants were aliquoted and stored at -80˚C until use.

Myelin extraction, purification, and pHrodo tagging

Myelin was extracted and purified from 3-month-old male and female C57BL/6J mice ($n=6$) using established protocols [1]. Each brain was quickly extracted and homogenized in ice-cold myelin lysis buffer (10 mM HEPES, 5 mM EDTA, 0.3 M sucrose with protease inhibitor). Homogenized lysate was transferred to ultra-clear centrifuge tubes (Beckman Coulter, 344057) and ice-cold 0.32 M sucrose was layered underneath followed by 0.85 M sucrose underneath both layers. Tubes were then centrifuged at 75,000 g at 4˚C for 30 min with low acceleration and deceleration. Myelin was collected at the 0.32 M and 0.85 M sucrose interfaces, then resuspended in 5mL of water and spun at 12,000 g at 4˚C for 10 min with high acceleration and deceleration three times. The purified myelin was then resuspended in PBS and adjusted to a concentration of 1 mg/mL. Myelin was stored at -80˚C until use.

A portion of the myelin to be used for phagocytosis experiments was tagged with the pH-sensitive pHrodo Red, succinimidyl ester (Thermo, P36600) according to manufacturer's instructions. Residual untagged pHrodo was removed through vortexing in 1mL methanol followed by centrifugation at max speed. This step was repeated until the supernatant turned clear. pHrodo-tagged myelin was then washed three times in PBS and finally resuspended at the original volume to achieve 1 mg/mL. The pHrodo-tagged myelin was then stored at -80˚C until use.

Aggregated fibrillar Aβ1–42 preparation and pHrodo tagging

Lyophilized human $A\beta_{1-42}$ (Anaspec, AS-20276, 1 mg) was brought to room temperature and then reconstituted in 100mM NaOH and gently vortexed for 1 min until dissolved. The solution was then neutralized and brought to a concentration of 1 mg/mL using 1x PBS. The fibrillization process was carried out immediately after on half the solution by further dilution to 0.5 mg/mL in 1x PBS. The diluted proportion was incubated at 37 °C for 24 h with shaking. The undiluted remainder was stored at -80 °C.

A portion of the fibrillar $A\beta_{1-42}$ to be used for phagocytosis experiments was tagged with the pH-sensitive pHrodo Red, succinimidyl ester (Thermo, P36600) according to manufacturer's instructions. The pHrodo-tagged fibrillar $A\beta_{1-42}$ was resuspended to a final concentration of 1 mg/mL and stored at -80˚C until use.

Western blotting

Homogenized brain lysates were prepared as described above, then protein concentrations were measured using the Pierce BCA Protein Assay kit (Thermo Scientific) according to the manufacturer's protocol. Proteins were denatured at 95˚C for 10 min in a solution containing 1x NuPAGE sample reducing agent (Invitrogen) and 1x NuPAGE LDS sample buffer (Invitrogen). 20 µg of total protein per sample were loaded into NuPAGE 4–12% Bis-Tris gels and run at a constant 160 V for 1 h in 1x MES Running Buffer (Thermo Scientific). Proteins were transferred onto 0.45-µm Immobilon-FL PVDF membranes (Millipore) in 1x Transfer Buffer containing methanol overnight at 4 °C. Membranes were washed in 0.1% Tween-20 in PBS, blocked in Intercept Blocking Buffer (LI-COR, 927-70001) for 1 h at room temperature, and incubated with the appropriate primary antibody overnight at 4 °C. The following primary antibodies were used: MBP (1:2000, Abcam, ab7349), dMBP (1:1000, Millipore, AB5864), CNPase (1:500, Abcam, ab6319), SMI-31 (1:1000, Biolegend, 801602), SMI-32 (1:1000, Biolegend, 801702), and loading control β-actin (1:20000, Sigma, A1978). Membranes were washed three times before incubation with the corresponding near-IR

secondary antibodies (1:5000, LI-COR) in blocking buffer for 1 h at room temperature. Membranes were washed three times and visualized using an Azure 600 western blot imager (Azure Biosystems). Images were analyzed with Image Studio software (LI-COR) to measure band densiometry and normalized to loading controls.

Immunohistochemistry

30-µm free-floating sections were prepared as described above, then washed and permeabilized in 0.1% Triton-X100 in PBS followed by antigen retrieval using 10mM sodium citrate, pH 6.0 at 95 °C for 10 min. Sections were allowed to cool to room temperature, washed in PBS, and blocked in 10% goat serum containing 0.3% Triton-X100 in PBS for 1 h at room temperature with rotation. Sections were then incubated with combinations of the following primary antibodies in blocking buffer overnight at 4 °C: Iba-1 (Wako, 019–19741), GFAP (Thermo Scientific, 13–0300), MBP (Abcam, ab7349), Olig2 (Millipore, AB9610), CC1 (Millipore, OP80), PLP (Novus Biologicals, NB100-74503), CD68 (Bio-rad, MCA1957). All primary antibodies were used at a dilution of 1:500. Sections were washed three times before incubation with the corresponding Alexa Fluor-conjugated species-specific secondaries (1:1000, Thermo Scientific) in blocking buffer for 1 h at room temperature. Staining for CD68 followed a modified protocol that included extending the primary and secondary incubations two-fold. Lipofuscin was visualized by exploiting autofluorescence using 488 nm excitation. Sections were washed three times, mounted on slides, and imaged using a Leica DMi8 inverted fluorescence microscope.

Images were collected at 20x magnification from 2 randomly selected areas within the striatum per section, 3 sections per animal, 4–5 animals per genotype at each age. Iba-1 was quantified as total cellular counts, percentage of stained area, and cell size. GFAP was quantified as percentage of stained area normalized to the total amount of myelin (via MBP) staining to account for section-to-section variability in myelin as astrocytes preferentially localize to the white matter. MBP was quantified as percentage of stained area and as percent fragmented using size exclusion to only quantify the smaller fragments as a percent of total MBP area. Olig2 and CC1 were quantified as total cellular counts. Oligodendrocyte precursor cells were defined as cells with single positivity of Olig2. Mature oligodendrocytes were defined as cells that had double positivity for Olig2 and CC1 using colocalization analysis. All analyses were conducted using Fiji (ImageJ) and the plug-ins included.

Electron microscopy

Mice at 12- and 18-months of age were perfused with ice-cold PBS. Brains were extracted and then immediately fixed in a 3% glutaraldehyde in 0.1 M cacodylate buffer solution, pH 7.4 at 4˚C. Fixed brains were then sectioned coronally (30-µm thick) using a Leica vibratome. Striatal regions were further isolated into 3 mm x 3 mm regions of interest in the same fixative solution. After primary fixation, samples were washed in 0.1 M cacodylate buffer and postfixed in 1% osmium tetroxide in 0.1 M cacodylate buffer for at least 1 h. The fixative solution was removed. Sections were rinsed in 0.1 M cacodylate buffer before being dehydrated via a series of graded alcohols from 70 to 100%. After two changes into 100% acetone, the sections were placed in a 50:50 mixture of acetone and EMbed 812 resin (Electron Microscopy Sciences) media overnight. The following day, sections were placed into pure EMbed 812 resin for at least 4 h followed by a final change into fresh resin. Samples were left to polymerize in a 60˚C oven for 12–18 h. Blocks were then thin-sectioned using a Diatome diamond knife (Electron Microscopy Sciences) at 70–90 nm (silver to pale gold using color interference), placed on nickel mesh grids, and dried on filter paper for a minimum of an hour. The sections were stained with uranyl acetate stain (Electron Microscopy Sciences) for contrast, dried, and viewed on a Tecnai Spirit TEM (FEI) equipped with an AMT CCD camera.

Images were collected at both 4800x and 9300x magnifications in 4–5 randomly selected regions/image per animal; 3 animals per genotype at each age. All analyses sampled > 150 axons per animal. The lower magnification images were used for axonal counts and characterization. The higher magnification images were used to quantify g-ratio and myelin thickness. Image analysis was carried out using MyelTracer software [32].

ELISAs

Homogenized white-matter lysates were prepared as described above. IGF-1, BDNF, and gal-3 concentrations were quantified using the following single analyte detection kits: Quantikine ELISA mouse/rat IGF-1 kit (R&D Systems, MG100), U-PLEX mouse BDNF kit (Meso Scale Diagnostics, K1526WK), and a sandwich ELISA Galectin-3 mouse kit (Invitrogen, EMLGALS3). Protein concentrations of cytokines including CXCL1, IL-1β, TNF-α, IL-5, and IL-6 were quantified by multiplex analyses using V-PLEX Proinflammatory Panel 1 mouse kit (Meso Scale Diagnostics, K15048D). All plates were prepared according to the manufacturer's protocol. The Meso Scale Diagnostics plates were read using the MESO QuickPlex SQ 120 instrument. All other plates were read on a Biotek Synergy H1 microplate reader using the appropriate wavelength absorbance. The multiplex ELISAs were evaluated using an increased sample size to account for the inherent variability over singleplex ELISAs.

Primary culture

Brains were extracted from P2-P4 pups and microdissected in 0.5% glucose in PBS on ice to remove the midbrain, meninges, and residual vasculature. Brain tissue was then gently triturated in ice-cold DMEM/F-12 (Gibco) using a p1000 pipet tip followed by a p200 pipet tip three times each before being filtered through a 70 µm nylon cell strainer and subsequently centrifuged at 400 x g for 8 min. Supernatant was removed, and the pellet was carefully resuspended in cell culture media containing: DMEM/F-12, 10% Defined FBS (Cytiva), 1x GlutaMAX (Gibco), 5% Penicillin/Streptomycin (Gibco), and 1x sodium pyruvate (Gibco). The suspension was then equally distributed into poly-d-lysine (PDL)-coated T75 flasks with 25mL of culture media and incubated at 37˚C with 5% CO_2. A full culture media change was performed 24 h after plating followed by half culture media changes every 3–5 days as needed. Microglia were harvested 10–13 days post-plating, determined by presence of mature cell populations, and placed in fresh media. Harvesting was performed by shaking at ~200 rpm at 37˚C for 2 h, followed by collection of media that was then spun down at 400 x g for 8 min. The supernatant was removed, and the cell pellet was resuspended in media. Cells were then plated onto PDL-coated Nunc 96-Well Optical-Bottom Plates (Thermo Scientific,165305) at a density of 35,000 cells/well for phagocytosis assays or PDL-coated Nunc 6-Well Plates (Thermo Scientific, 140675) at a density of 750,000 cells/well for RNA analysis. Microglia were allowed to rest in the incubator 18–24 h before use.

Phagocytosis assay

Cells previously plated on a 96-well plate were washed with serum-free culture media to remove debris, unattached cells, and residual serum. Fresh serum-free media was then added to the wells at a volume of 150µL for 3–4 h for serum starvation. pHrodo-tagged myelin or fibrillar Aβ, prepared as described above, was diluted in 50µL serum-free media adjusted to achieve concentrations ranging from 1 to 5 mg/mL and added to each well for a total of 200µL volume/well. The plate was then placed in the incubator and analyzed at 30-minute to 1-hour intervals over 6 total hours using a Biotek Synergy H1 microplate reader at an excitation and emission wavelength of 560 nm & 590 nm, followed by imaging on a Leica DMi8 fluorescent microscope at coordinates randomly preset before myelin treatments. Untreated cells, media only, and media with diluted pHrodo were used as normalization controls to account for background effects during absorbance measurement. Technical replicates (n=4–6 wells/treatment) were averaged together to give a single mean for each biological replicate. Biological replicates (n=3–4) were comprised of different groups of cells from either separate flasks or experiments.

RNA analyses

400µL TRIzol LS Reagent (Ambion) was added to brain tissue or primary microglial cells plated as described in phagocytosis assay, placed on an orbital shaker to incubate for 2 min, and a cell scraper was used to ensure all cells were collected. RNA was isolated using the RNeasy Plus Universal kit (QIAGEN, 73404) using the manufacturer's protocol. Isolated RNA was then quantified using a Nanodrop spectrophotometer. Samples with low-quality measurements (260/280 or 260/230 < 1.7) were repurified using the Clean & Concentrator-5 kit (Zymo Research, R1016). cDNA synthesis was then carried out from 500ng total RNA using the High-Capacity RNA-to-cDNA kit (Applied Biosystems) according to manufacturer's suggested thermocycler settings. RT-qPCR was then performed using Taqman Gene Expression assays (Applied Biosystems) for *Cd68* (Mm03047343_m1), *CtsL* (Mm00515597_m1), *Gns* (Mm00659592_m1), *Glb1* (Mm00515342_m1), *Lgals3* (Mm00802901_m1), *Hspa5* (Mm00517691_m1), and *Ddit3* (Mm00492097_m1) in 96-well plates on an Applied Biosystems QuantStudio 6 Flex Real-Time PCR system. Data was analyzed using QuantStudio software (Applied Biosystems) using the ΔΔCT method calculated with reference ΔCTs from non-treated samples for each genotype using *Gapdh* (Applied Biosystems, 4352339E) as a housekeeping gene. All samples were run in duplicate.

Statistical analyses

All statistical analysis and plotting of data was carried out using Graphpad Prism software (version 10.0.0). Experiments were sex-matched when possible, however no sex differences were observed, so male and female data are grouped for analysis. At least two independent experiments were performed for each analysis unless otherwise stated. Details of data measurement and collection are outlined under the relevant method. Specific statistical tests and other information applicable to the analyses are included in the figure legends.

Results

Trem2-deficiency exacerbates age-related myelin damage in the striatum

To explore the role of TREM2 in age-related myelin degeneration, we characterized myelin dynamics in the striatum of 6- to 18-months old wildtype C57BL/6J (WT) and Trem2$^{-/-}$ mice. We first analyzed total myelin area across age using immunohistochemistry for myelin basic protein (MBP), one of the most abundant proteins in myelin. We found WT striatum displayed increased MBP staining from 6- to 18-months but did not reach

significance (Fig. 1A-B). Interestingly, Trem2$^{-/-}$ mice showed increased MBP staining from 6-months to 12-months that plateaued by 18-months of age. There was no significant difference in the total area of myelin between the genotypes at any age. Since myelin fragments and splits as it degenerates, we asked if increased myelin fragmentation could account for the increased myelin area in Trem2$^{-/-}$ mice by quantifying the area comprised of fragmented myelin as a percent of total myelin area (Fig. 1A insets, 1C) [49, 58, 66]. The percent fragmentation in Trem2$^{-/-}$ mice significantly increased with age (Fig. 1C). However, in WT mice, increased fragmentation only became apparent at 18-months of age. Despite this, Trem2$^{-/-}$ mice contained significantly more fragmentation compared to WT mice at the later timepoints.

To confirm if protein levels of other structural components of myelin were likewise impacted by Trem2 and/or age, western blot analyses were performed using an antibody against 2′,3′-Cyclic-nucleotide 3′-phosphodiesterase (CNPase), a membrane-associated enzyme involved in myelin formation/maintenance [27]. WT mice exhibited age-related increases in CNPase with only the 18-month timepoint showing a significant increase compared to Trem2$^{-/-}$ mice (Fig. 1D-E). Myelin fragmentation was also confirmed using an antibody against degraded myelin basic protein (dMBP), which detects a pathologically exposed epitope of myelin (amino acids 81–87;QDENPVV). Age-related increases in myelin degradation were observed in both WT and Trem2$^{-/-}$ mice from 6- to 12-months of age. However, myelin damage in WT mice plateaued by 18-months of age, while damage

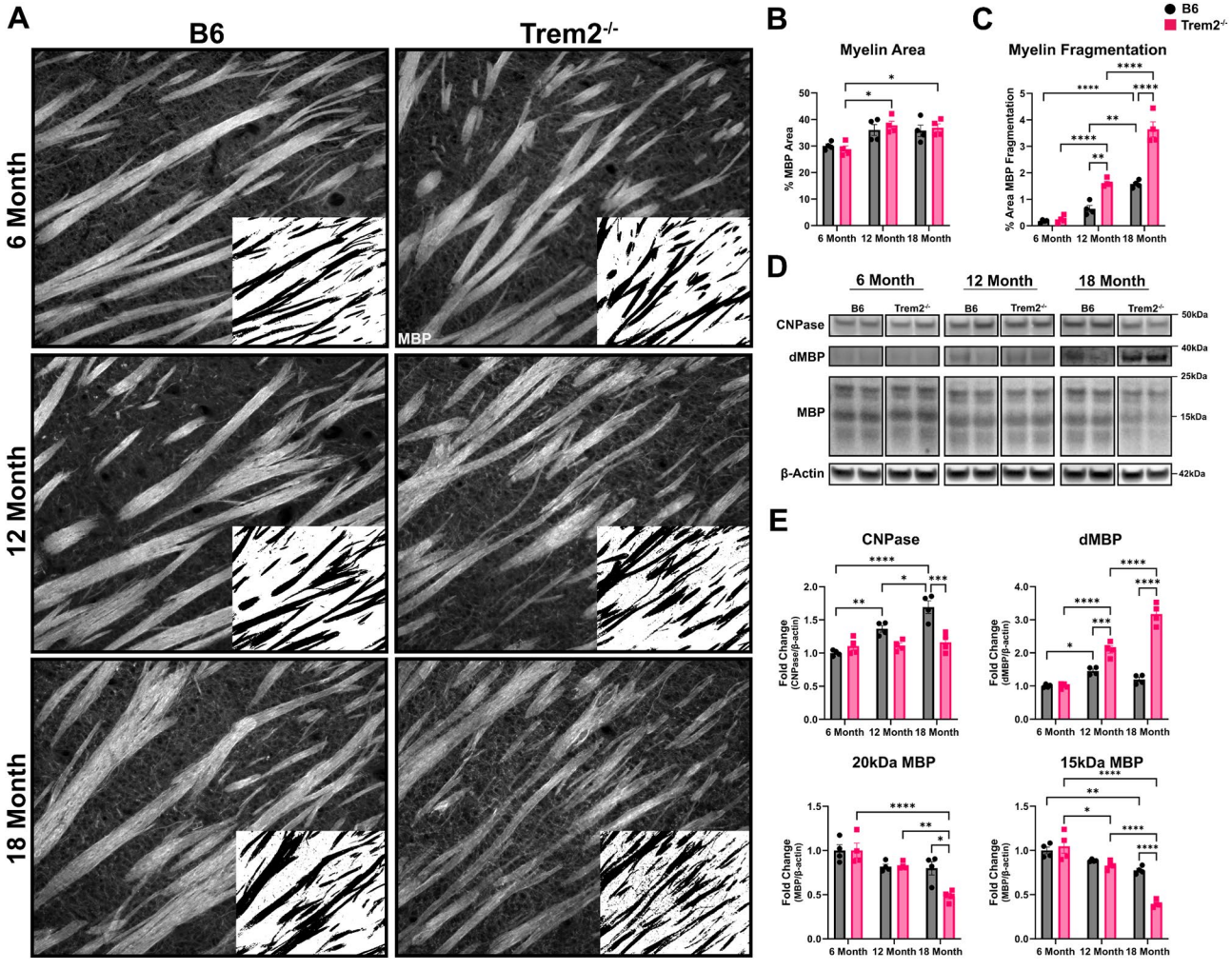

Fig. 1 Trem2-deficiency exacerbates age-related myelin damage in the striatum. (**A**) Representative fluorescent images of striatal white matter from 6-, 12-, and 18-month-old B6 and Trem2$^{-/-}$ mice stained for MBP (gray) with binary insets highlighting the fragmentation. (**B**) Quantification of MBP percent area and (**C**) fragmentation in 6-, 12-, and 18-month striatum. (**D**) Representative western blot analysis and (**E**) densiometric quantification of white matter proteins CNPase, dMBP, and MBP in white matter homogenates from 6-, 12-, and 18-month-old B6 and Trem2$^{-/-}$ mice. Immunoblot quantification was normalized to 6-month B6 samples. All experiments used $n = 4$ (equal males and females) per group. Two-way ANOVA with Tukey's post-hoc test (*$P < 0.05$, **$P < 0.01$, ***$P < 0.001$, ****$P < 0.0001$) was used for statistical analysis. Error bars represent SEM

in Trem2$^{-/-}$ mice continued to increase (Fig. 1D-E). In addition, Trem2$^{-/-}$ mice had significantly higher levels of myelin damage at both ages compared to WT mice.

As MBP exists in multiple isoforms ranging from 14 kDa to 21.5 kDa that are believed to have different roles in (re)myelination and cytoskeletal remodeling, we also evaluated two major isoforms of MBP to determine if any isoforms showed predominance [27]. Protein expression levels of the larger ~ 20 kDa MBP isoform, thought to correspond to early myelin development, showed an age-related reduction in Trem2$^{-/-}$ mice from 12- to 18-months of age [6]. At the 18-month timepoint, Trem2$^{-/-}$ mice had significantly lower concentrations of the ~ 20 kDa MBP isoform compared to WT mice (Fig. 1D-E). The second smaller MBP isoform of ~ 15 kDa has been suggested to be involved in remyelination [6]. Trem2$^{-/-}$ mice displayed a progressive reduction in levels of the ~ 15 kDa MBP isoform from 6- to 18-months of age, while WT mice only showed decreased levels at 18-months of age (Fig. 1D-E). At the 18-month timepoint, Trem2$^{-/-}$ mice had significantly less ~ 15 kDa MBP isoform compared to WT mice. It has been reported that Trem2 deficiency results in exacerbated myelin degeneration in models of MS, neuromyelitis optica syndrome disorder, and AD in the corpus callosum, optic tracts, and frontal lobe [8, 52, 64, 70]. Our results are consistent with these reports; however, we show Trem2 deficiency does not exacerbate cortical white matter degeneration during aging (Fig. 1SA-C). Together, these results demonstrate age-related myelin damage in the striatum that is aggravated in the absence of Trem2.

Reduction of myelin integrity, accumulation of myelin debris, and axonal damage persists with age in striatum of Trem2-deficient mice

To probe white matter changes at a more granular level, transmission electron microscopy was performed on striatum from mice at 12- and 18-months of age (Fig. 2A). General myelin integrity was assessed by measuring the ratio of the inner axonal diameter relative to the total fiber diameter (including myelin sheath), known as the g-ratio. A significant decrease in g-ratio, indicating improved myelin integrity, was observed in WT mice between 12- and 18-months of age, while no change was seen in Trem2$^{-/-}$ mice (Fig. 2B). However, compared to WT mice, there were significantly higher g-ratios observed at both ages in Trem2$^{-/-}$ mice (Fig. 2B). G-ratio often gives an incomplete picture and fails to account for other pathological features that may skew ratios in either direction, so we also assessed myelin thickness. Myelin thickness measurements showed similar results as the g-ratio, but further revealed an age-related decline in myelin thickness in both WT and Trem2$^{-/-}$ mice (Fig. 2C).

We next plotted both g-ratio and myelin thickness as a function of axon diameter to provide clarity on the level of myelination for individual axons and the correlations between genotypes at each age. Of note, there were no significant differences in axon counts or diameters observed between groups at either age (Fig. S2A-B). At 12-months of age, Trem2$^{-/-}$ mice showed a relatively higher g-ratio that became more pronounced across the mid- to large-diameter axons compared to WT mice. (Fig. 2D). Likewise, reduced myelin thickness was observed in Trem2$^{-/-}$ mice compared to WT mice (Fig. 2E). While there was minimal difference in the trends of either metric between the genotypes by 18-months of age, the Trem2$^{-/-}$ mice had a denser group of high g-ratio, low myelin thickness axons at smaller diameters relative to WT mice (Fig. 2D-E). Across age, the g-ratio in Trem2$^{-/-}$ mice remained relatively unchanged with a progressive reduction in the myelin thickness of small-diameter axons (Fig. S2E-F). However, WT mice showed a marginal shift toward higher g-ratio accompanied by a slight reduction in the myelin thickness of small- to mid-diameter axons (Fig. S2C-D). A common morphological characteristic of remyelination is presence of axons with thin myelin sheaths that display an increase in g-ratio [20, 53]. Further, reported data indicate remyelination preferentially begins with small- to mid-diameter axons [20]. Both features were observed in WT mice (Fig. S2C-D), indicating some level of remyelination in the smaller axons. Thus, Trem2 deficiency negatively impacts myelin recovery.

Given that persistent white matter damage can lead to ultrastructural changes in the myelin sheath [12, 58, 66], we classified prominent pathological features and quantified them as a percentage of the total axons surveyed (Fig. 2F-G). Strikingly, even at 12-months of age, upwards of 60% of the axons in Trem2$^{-/-}$ mice exhibit pathology. Axons were initially categorized as intact myelinated or unmyelinated to determine general levels of demyelination from 12- to 18-months of age. Trem2$^{-/-}$ mice on average lost ~ 7% more intact myelinated axons than WT mice, however both genotypes had a similar ~ 5% increase in unmyelinated axons. Next, we quantified axons with vesiculation or degenerating myelin sheaths. Vesiculated sheaths form during the process of demyelination as a consequence of de-adhesion of myelin from the membrane [49, 66]. These vesicles are linked to swelling that continues to separate the sheath from the axon, ultimately leading to degeneration of the sheath [49, 66]. Only minor changes in the proportion of vesiculated sheaths were seen between the ages in either genotype, but by 18-months of age, Trem2$^{-/-}$ mice had nearly double the proportion of vesiculated sheaths relative to WT mice. The rate of sheath degeneration was also similar in WT and Trem2$^{-/-}$ mice, but by 18-months of age,

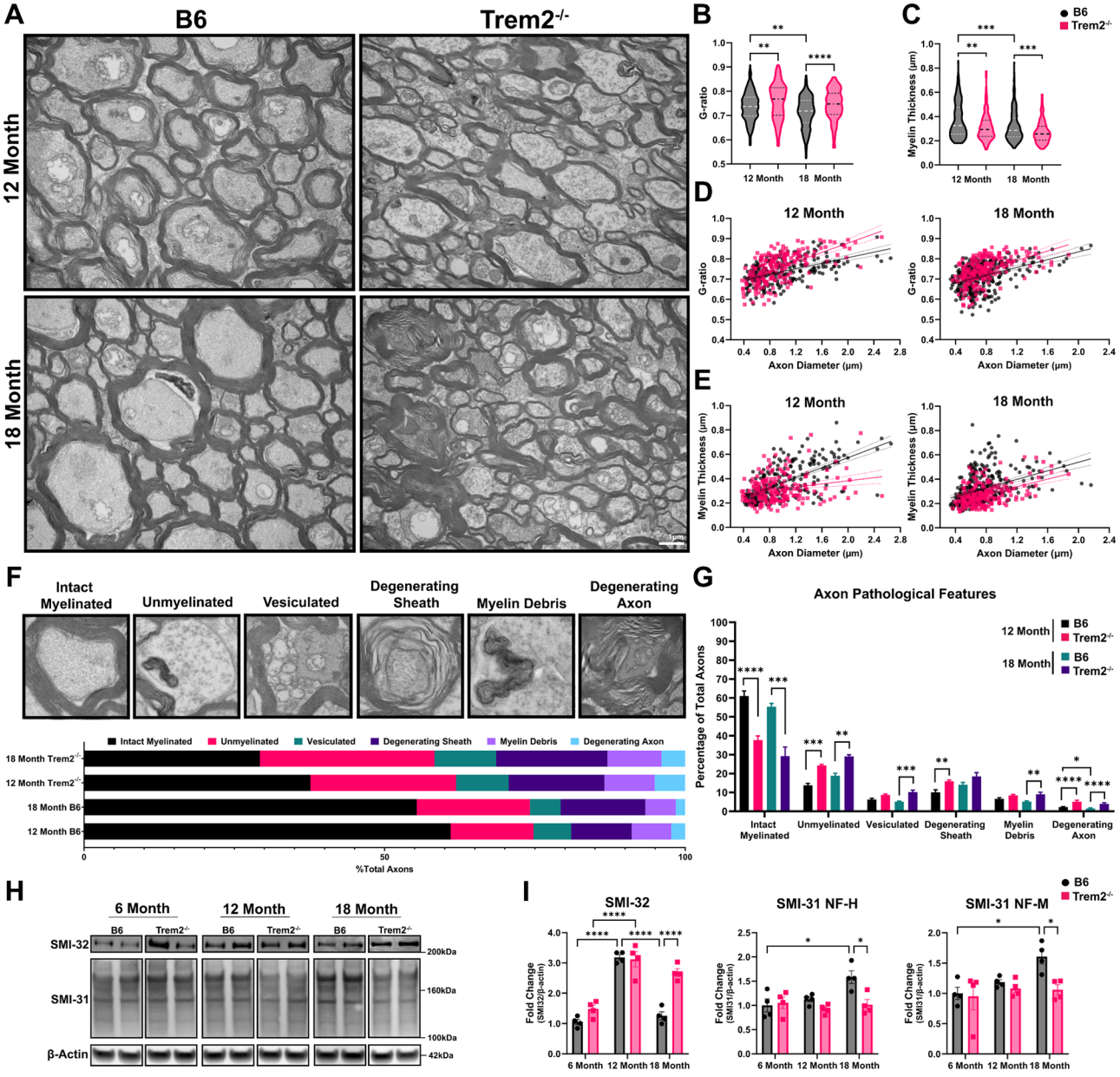

Fig. 2 Reduction in myelin integrity, myelin debris accumulation, and axonal damage persists with age in striata of Trem2-deficient mice. (**A**) Representative transmission electron micrographs of striatal white matter from 12- and 18-month-old B6 and Trem2$^{-/-}$ mice (9300x). Quantification of g-ratio (**B**) and myelin thickness (**C**) in striatal white matter at 12- and 18-months ($n = 2$–3 (all male) per group, 200–250 axons per animal). Kruskal-Wallis with Dunn's post-hoc test (**$P < 0.01$, ***$P < 0.001$, ****$P < 0.0001$) was used for statistical analysis. Data plotted as median and interquartile range. Associations of g-ratios (**D**) and myelin thickness (**E**) to axonal diameters in 12- and 18-month-old mice. Bars represent medians. Dotted lines represent 95% confidence interval. (**F-G**) Characterization and quantification of indicated pathological features observed in axons as a percentage of total axons in 12- and 18-month B6 and Trem2$^{-/-}$ mice. Two-way ANOVA with Tukey's post-hoc test (*$P < 0.05$, **$P < 0.01$, ***$P < 0.001$, ****$P < 0.0001$) was used on transformed values. (**H**) Representative western blot analysis and (**I**) densiometric quantification of axonal proteins SMI-31 and SMI-32 in white matter from 6-, 12-, and 18-month-old mice ($n = 4$ (equal males and females) per group). Quantification was normalized to 6-month B6 samples. Two-way ANOVA with Tukey's post-hoc test (*$P < 0.05$, ****$P < 0.0001$) was used for statistical analysis. Error bars represent SEM

Trem2$^{-/-}$ mice maintained more degenerating sheaths than WT mice. Degenerating sheaths can contribute to production of myelin debris, so we also quantified the amount of myelin debris. The percentage of myelin debris progressively worsened in Trem2$^{-/-}$ mice, in contrast to a slight decrease in WT mice, leading to a comparative two-fold increase in the level of debris in Trem2$^{-/-}$ mice. Lastly, we analyzed the number of degenerating axons, which are marked by the appearance of darkened axons due to high electron density as a result of a collapse in

microtubule organization [58]. We found that the presence of degenerating axons was consistently higher in Trem2$^{-/-}$ mice and progressively worsened, while WT mice exhibited a slight decrease.

Chronic demyelination and/or inflammation can lead to and exacerbate axonal damage [49, 52, 65]. Since we observed unresolved, persistent demyelination coupled with a larger comparative increase in proportions of ultrastructural pathological features in Trem2$^{-/-}$ mice, we were prompted to investigate axonal integrity. Neurofilaments serve as integral structural components in axons and are present in variably phosphorylated and nonphosphorylated forms of low, medium, and high molecular weight where the latter is classically used to identify damaged and demyelinated axons. Using western blot analyses to quantify expression of both phosphorylated (SMI-31) and nonphosphorylated (SMI-32) neurofilaments, we observed increases in SMI-32 in both WT and Trem2$^{-/-}$ mice from 6- to 12-months of age. Curiously, SMI-32 returned to baseline levels in WT mice, and this was accompanied by an increase in SMI-31 at 18-months of age (Fig. 2H-I). The mechanisms orchestrating axonal repair are not entirely clear; however, studies modulating TREM2 activation in MS models report similar recoveries in SMI-32, thus implicating a more direct role for TREM2 in facilitating the repair of axonal damage [10, 62]. Further, the fluctuations in SMI-32 mirror other changes observed including the reduction in dMBP (Fig. 1D-E) and presence of degenerating axons (Fig. 2F-G). Together, these observations suggest absence of Trem2 leads to persistent axonal damage in the striatum.

Trem2 deficiency alters striatal glial response and shifts oligodendrocyte populations to predominantly non-mature phenotypes

Aging and Trem2 deficiency have both been shown to have a pronounced impact on glial numbers and function which could contribute to myelin degeneration [55]. Thus, we investigated whether the chronic myelin damage observed during aging in Trem2 deficiency also coincides with alterations in striatal glial populations. Using immunohistochemistry (Fig. 3A-B), we quantitated microglia, astrocytes, and oligodendrocytes.

We observed a smaller population of IBA1^{+} microglia in Trem2$^{-/-}$ mice than in WT mice at both ages; however, by 18-months of age, there was an age-related decrease in both genotypes (Fig. 3C). This observation contrasts with other studies that report age-related increases in microglia, particularly in white-matter regions such as the corpus callosum and cerebellum [52, 57]. We also detected an increase in microglia in the corpus callosum of our WT mice (Fig. S1D-E). In support of a decreasing microglial population in the striatum with age, other reports have similarly shown that age-related increases are not uniform and can decrease in regions like the substantia nigra and striatum [40, 59]. As TREM2 is also essential for activation, migration, and expansion of microglia in response to demyelination and aging [8, 10, 52, 65], microglial activation states may additionally influence the regional differences. To investigate the effect of TREM2 on the microglial response in the striatum, we assessed their activation using measures of the area of IBA1^{+} cell bodies and number of CD68^{+} cells (Fig. S3A-C). At 12-months of age, WT microglia were on average larger than their Trem2-deficient counterparts, indicating some level of activation, and by 18-months of age these differences diminished (Fig. S3B). Consistent with increased activation at 12-months of age, there was a larger number of CD68^{+} WT microglia, localized predominantly alongside the white matter tracts, that similarly diminished by 18-months of age (Fig. S3A, C). The apparent activation at 12-months of age that dissipates by 18-months of age coincides with pathology and is congruent with an initial expansion and subsequent reduction in the microglial population. This suggests that TREM2 promotes a region-specific microglial response to white matter damage and subsequent phagocytic activation during age-related degeneration.

To account for potential changes in the presence of fibrous astrocytes that preferentially localize to the white matter, GFAP^{+} area was normalized to MBP^{+} area. WT mice exhibited an age-related increase in white matter-associated GFAP^{+} astrocytes that was significantly elevated compared to Trem2$^{-/-}$ mice by 18-months of age (Fig. 3D). Of note, GFAP-positivity is commonly used to assess astrocyte reactivity. The lack of astrocytes in Trem2-deficient white matter implies that, in the context of aging and/or degenerating white matter, TREM2 influences astrocyte activation and/or recruitment.

To assess oligodendrocyte cell populations, oligodendrocyte precursor cells (OPCs) were defined as Olig2^{+}CC1^{-} cells, while mature oligodendrocytes were identified as Olig2^{+}CC1^{+} cells. The number of OPCs decreased in WT mice from 12- to 18-months, but no statistical differences were observed between the genotypes (Fig. 3E). The stalled myelin loss and partial remyelination observed in WT mice suggests that OPC differentiation led to the reduced OPC populations. We found no correlative increase in the mature oligodendrocyte population at 18-months of age in WT mice, however the number of mature oligodendrocytes in Trem2$^{-/-}$ mice declined by 18-months of age and was significantly lower than WT mice (Fig. 3F). Given this, we infer cell death likely also occurred in WT mice sometime after 12-months of age but recovered by 18-months of age. This may also explain the visual shift in Olig2^{+} cells from outside the white matter tracts at 12-months

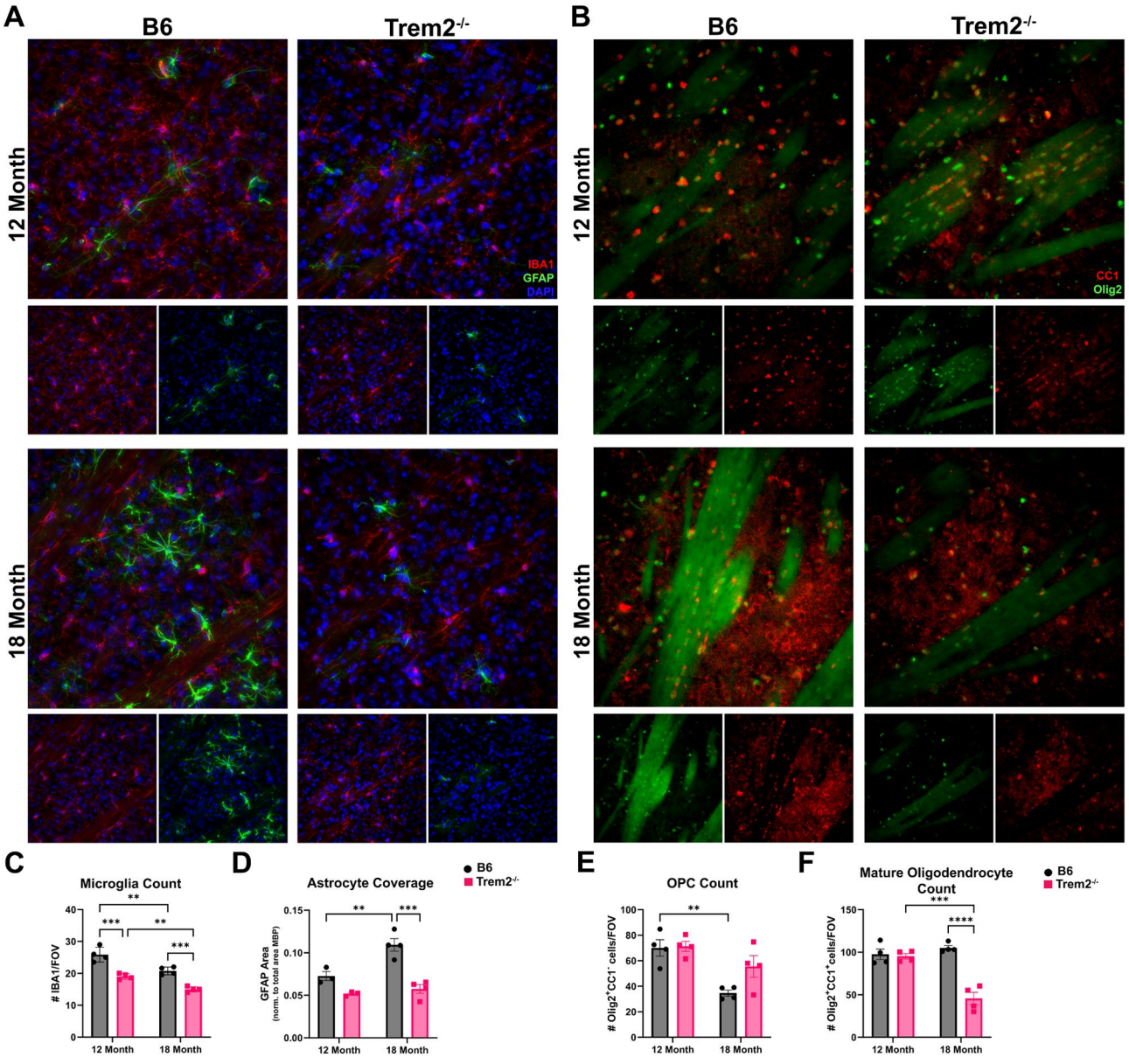

Fig. 3 Trem2-deficiency alters striatal glial numbers and shifts oligodendrocyte populations to predominantly non-mature cells. (**A**) Representative fluorescent images of microglia (IBA1; red) and astrocytes (GFAP; green) and (**B**) of total oligodendrocytes (Olig2; green) and mature oligodendrocytes (CC1; red) in the striatum of 12- and 18-month-old B6 and Trem2$^{-/-}$ mice (40x). (**C-D**) Quantification of microglia and astrocytes in 12- and 18-month-old B6 and Trem2$^{-/-}$ mice ($n=4$). Number **(C)** of IBA1^{+} microglia and percent area (**D**) of GFAP^{+} astrocytes per FOV. **(E-F)** Quantification of oligodendrocytes in 12- and 18-month-old B6 and Trem2$^{-/-}$ mice ($n=4$). Number of Olig2^{+}CC1^{-} cells (**E**) and Olig2^{+}CC1^{+} cells (**F**) for oligodendrocyte precursor and mature cells, respectively. Two-way ANOVA with Tukey's post-hoc test (*$P<0.05$, **$P<0.01$, ***$P<0.001$, ****$P<0.0001$) was used for statistical analysis. Error bars represent SEM

of age to largely within the tracts, with CC1-positivity, at 18-months of age in WT mice, while the opposite shift was observed in Trem2$^{-/-}$ mice. This implies TREM2 may impact oligodendrocyte survival and/or recruitment and differentiation.

Trem2 deficiency promotes dysfunctional signaling associated with impaired OPC differentiation and maturation in the striatum

Remyelination occurs via the process of oligodendrogenesis, which is orchestrated by migration of OPCs to areas of damage, proliferation of these OPCs, and subsequent differentiation and maturation into myelinating oligodendrocytes [19]. Oligodendrogenesis is driven by a fine-tuned interplay of cytokines and trophic factors

that mediate each step and are released predominantly by microglia and astrocytes (Fig. 4A) [51]. Since we observed that Trem2 deficiency reduced the mature oligodendrocyte population and altered microglia and astrocyte numbers in striatal white matter, we asked whether these alterations were accompanied with or caused by impairment in the signaling that promotes oligodendrogenesis.

Cytokines supporting migration showed age-related changes in CXCL1 and IL-1β concentrations and *Cxcl12* expression in WT and Trem2$^{-/-}$ mice, but, other than IL-1β, these migration factors did not differ between the two genotypes at any age (Fig. 4B-D). Next, we investigated signals associated with proliferation which also showed little change in the absence of Trem2 other than an increase in TNF-α concentrations in WT mice at 18-months of age (Fig. 4E-G). As CXCL1, IL-1β, and TNF-α are involved in OPC migration and proliferation, the increases were likely driven in response to alterations in the OPC population and not TREM2 [45, 47]. Their release and subsequent increase parallel the comparable OPC counts between the genotypes at 12 months and the reduction in WT mice by 18 months (Fig. 3E). Together, this suggests TREM2 has no overt effect on OPC migration or proliferation. Lastly, we examined differentiation and maturation signaling, which revealed Trem2-dependent changes in BDNF, IGF-1, and Gal-3. Compared to Trem2$^{-/-}$ mice, BDNF concentrations were higher in WT mice at all ages (Fig. 4H). Similarly, IGF-1 concentrations were higher in WT mice at 12- and 18-months of age (Fig. 4I). Gal-3 concentrations increased with age in both WT and Trem2$^{-/-}$ mice, but WT mice showed larger comparative increases compared to Trem2$^{-/-}$ mice (Fig. 4J). Interestingly, these results suggest, following the onset of more pronounced age-related myelin damage, that Trem2$^{-/-}$ microglia lack a sufficient response rather than an absence of one. This indicates differentiation and maturation signaling is influenced by TREM2.

Deficits in phagocytosis of myelin are volume- and time-dependent in Trem2-deficient microglia

Reports have shown that TREM2 is a crucial regulator of various processes involved in demyelination, including lipid sensing and phagocytosis [8, 10, 52, 64]. A critical step in proper remyelination is the removal of myelin debris by phagocytes. Without adequate and efficient debris clearance, oligodendrogenesis is hindered and (re)myelination remains incomplete [35, 36]. To further explore TREM2-dependent defects in the microglial response to myelin, we evaluated multiple steps in phagocytosis from uptake to processing using a phagocytosis assay with WT or Trem2$^{-/-}$ primary microglia. Functional outcomes of TREM2 are known to have both a context- and stage-dependent response, where in certain situations it is beneficial and others detrimental [4, 31, 39, 40]. Due to this, we first sought to establish if microglia uptake of myelin differed from another common aging/degenerative element such as amyloid beta (Aβ). Primary microglia isolated from WT and Trem2$^{-/-}$ mice were treated with either 5 μg/mL myelin or fibrillar $A\beta_{1-42}$, and uptake was assessed via fluorescence over six hours (Fig. 5A). Trem2$^{-/-}$ microglia showed a clear deficit in myelin uptake at all timepoints post-treatment compared to WT microglia (Fig. 5B). However, we did not observe significant differences in the uptake of fibrillar $A\beta_{1-42}$ between the two genotypes (Fig. 5C).

Since TREM2 has also been linked to regulation of lysosomal function and lipid and cholesterol metabolism, we sought to dissect the role TREM2 plays during the processing and subsequent metabolism of myelin debris by analyzing expression of genes associated with microglial activation or lysosomal activity (*Cd68*, *CtsL*, *Gns*, *Glb1*, *and Lgals3*) [8, 21, 48]. Myelin treatment of primary Trem2$^{-/-}$ microglia led to downregulation of the activation- and lysosomal-linked genes, whereas these genes were upregulated in WT microglia (Fig. 5D). When querying these genes in Aβ-treated microglia, only *CtsL* expression was significantly reduced in Trem2$^{-/-}$ microglia compared to WT microglia (Fig. 5D). This finding supports our observation that TREM2-deficient microglia can uptake Aβ similarly to WT microglia and suggests there are negligible deficits in processing Aβ. Furthermore, this directed transcriptomic analysis suggests that the dysfunctional response of Trem2-deficient microglia may largely be a myelin/lipid-specific deficit.

The endoplasmic reticulum (ER) and the unfolded protein response (UPR) are implicated in lipid metabolism and homeostasis [28]. Since our in vitro data revealed a myelin-specific deficit in uptake and processing for TREM2-deficient microglia, we queried expression of genes related to the ER/UPR response (*Hspa5* and *Ddit3)*. *Hspa5* expression is connected to positive regulation of pathways associated with survival, while *Ddit3* expression drives pro-apoptotic pathways [28]. After treatment with myelin, Trem2$^{-/-}$ microglia failed to upregulate *Hspa5* but not *Ddit3*, whereas WT microglia showed the opposite trend (Fig. 5D). As seen with the other gene interrogations, Aβ treatment did not reveal any differences in the ER/UPR response of microglia between the two genotypes. This suggests impaired ER/UPR responses contribute to the overall dysfunction of Trem2-deficient microglia during demyelination.

A sustained microglial response is essential to adequately address persistent demyelination and mounting levels of debris. As our in vivo data showed persistent demyelination and increased myelin debris in striatal white matter of TREM2-deficient mice, we investigated whether the inability of TREM2-deficient microglia to confront and resolve white matter damage

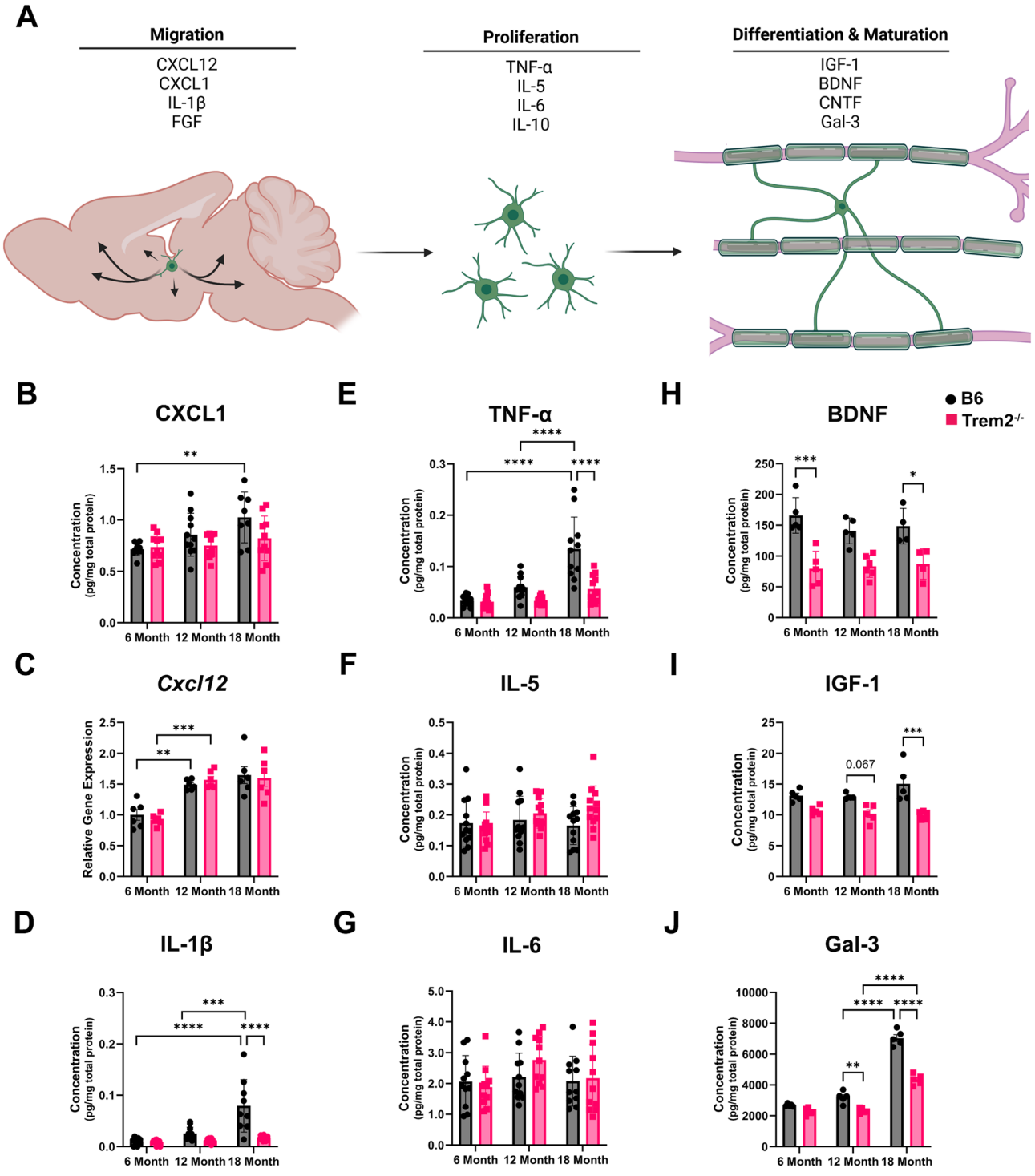

Fig. 4 Trem2-deficiency promotes dysfunctional signaling associated with impaired differentiation and maturation during oligodendrogenesis in the striatum. (**A**) Illustration of general steps in oligodendrogenesis and examples of cytokines and tropic factors involved. (**B-I**) Analyses of expression levels of oligodendrogenesis-associated cytokines and trophic factors in 6-, 12-, and 18-month-old B6 and Trem2$^{-/-}$ mice. (**B-D**) Quantification of signaling involved in migration. Multiplex ELISA analysis of CXCL1 and IL-1β ($n = 8$–12 mice) and qPCR analysis of *Cxcl12* ($n = 5$–6 mice). (**E-G**) Quantification of signaling involved in proliferation. Multiplex ELISA analyses of TNF-α, IL-5, and IL-6 ($n = 8$–12 mice). (**H-J**) Quantification of signaling involved in differentiation and maturation. ELISA analyses of BDNF, IGF-1, and Gal-3 ($n = 5$–6 mice). Two-way ANOVA with Tukey's post-hoc test (*$P < 0.05$, **$P < 0.01$, ***$P < 0.001$, ****$P < 0.0001$) was used for statistical analysis. Error bars represent SEM

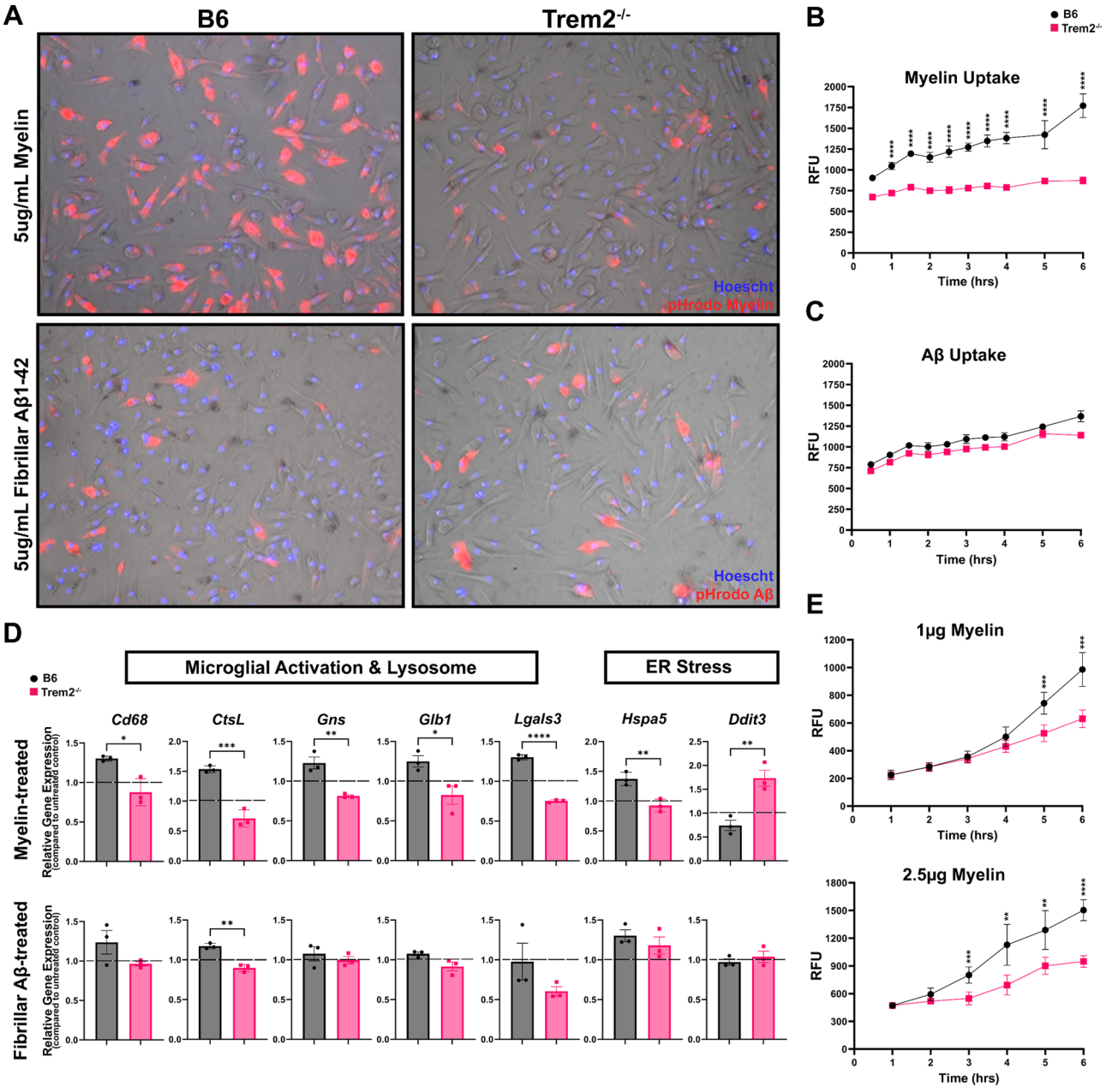

Fig. 5 Deficits in microglial phagocytosis are volume- and time-dependent in Trem2-deficient microglia. (**A**) Representative images of B6 and Trem2$^{-/-}$ primary microglia treated with 5 μg/mL of pHrodo-conjugated myelin (red) or fibrillar Aβ_{1-42} (red) at 6 h. Cells were counterstained with Hoescht (nuclei, blue). Black areas show myelin or Aβ_{1-42} that has not been taken up. (**B-C**) Fluorescent quantification in relative fluorescent units (RFU) of pHrodo-labeled myelin (**B**) or fibrillar Aβ_{1-42} (**C**) uptake by B6 and Trem2$^{-/-}$ primary microglia. Measurements were taken every hour over 6 h. Data were analyzed by repeated measures ANOVA with Sidak's correction (*$P < 0.05$, **$P < 0.01$, ***$P < 0.001$, ****$P < 0.0001$). Error bars represent SD. (**D**) qPCR analysis of microglial activation, lysosomal, and ER stress genes relative to untreated genotype controls (dotted line) at the end of the 6-hour treatment. Student's t-test (*$P < 0.05$, **$P < 0.01$, ***$P < 0.001$, ****$P < 0.0001$) was used for statistical analysis. Error bars represent SEM. (**E**) Fluorescent quantification in RFU during a phagocytosis assay of increasing concentrations of myelin (1 mg and 2.5 mg) over a 6-hour treatment. Repeated measures ANOVA with Sidak's correction (**$P < 0.01$, ***$P < 0.001$, ****$P < 0.0001$) was used for statistical analysis. Error bars represent SD

is influenced by the duration of phagocytosis, the volume of myelin debris, or both. To do so, we tested the capacity of microglia to confront varying debris loads over time. At the lower myelin concentration (1 μg/mL), Trem2$^{-/-}$ microglia remained relatively competent with a comparative reduction in uptake only occurring five hours into the assay, whereas the higher myelin concentration (2.5 μg/mL) led to an observable reduction in uptake at three hours (Fig. 5E). Exploration of concomitant alterations in the lysosomal and ER/UPR

response as a function of myelin debris volume revealed Trem2$^{-/-}$ microglia treated with the lower myelin concentration (1 μg/mL) only altered expression of the ER/UPR gene *Ddit3* (Fig. S4A-B). However, at the higher myelin concentration (2.5 μg/mL), Trem2$^{-/-}$ microglia exhibited similar trends as the 5 μg/mL analysis in all genes but *Glb1* (Fig S4A-B). Taken together, these data suggest that Trem2-deficient microglia can become both progressively overwhelmed when confronting low levels of myelin debris over time and/or increasingly dysfunctional when confronting mounting levels of myelin debris.

Discussion

Recent aging studies have identified white matter regions such as the cerebellum, corpus callosum, and striatum as particularly vulnerable to aging [12, 13]. Additionally, a recent study revealed while there is a shared set of aging signatures across white matter regions, there are highly compartmentalized regional effects that confer susceptibility to degenerative diseases [26]. Likewise, the functional outcome of TREM2 activity is also highly contingent on region and pathological context [4, 31, 39]. Here, we explored how TREM2 modifies age-related myelin degeneration in the striatum. We found a robust level of myelin damage and demyelination evident early in Trem2$^{-/-}$ mice that persisted with age. While we also observed age-related damage in WT mice, it was less pronounced and progressed more slowly. These data corroborate other reports of exacerbated myelin degeneration in Trem2-deficient models and further validate Trem2-dependent protection during aging and in the striatum. Importantly, in many metrics of damage measured, the increases seen in WT mice by 18-months were not significantly different than the levels observed in Trem2$^{-/-}$ mice at 12-months. This indicates the absence of TREM2 accelerates the onset of age-related degeneration. WT mice also show some level of recovery from both axonal and myelin damage. Additionally, there were comparable levels of cortical white matter damage between the genotypes. Together, these observations suggest that the Trem2-mediated outcomes could be region-dependent and potentially striatum-specific.

Prior work has documented that age-related decreases in remyelination efficiency are due to impaired OPC recruitment and differentiation [14, 61]. Proteomic analysis of aging OPCs indicates an increasing inability to respond to signaling during oligodendrogenesis [16]. Importantly, modulation of TREM2 activity can lead to improved remyelination [10, 65]. Moreover, at sites of demyelination in models of MS and AD, Trem2-deficient microglia have been shown to secrete less neurotrophic factors [52, 64]. We sought to provide further insight into which aspects of remyelination TREM2 plays a role. We found no indication that TREM2 mediates OPC migration and proliferation signaling in the striatum, indicating that any impact is likely age related.

Remyelination induced by oligodendrocyte demyelination and/or cell death typically proceeds in two ways: OPCs are triggered to migrate and differentiate, or surviving oligodendrocytes are signaled to remyelinate [23, 53]. Our data indicate that the mature oligodendrocyte deficit in Trem2$^{-/-}$ mice was largely due to the inability to initiate signaling to promote OPC differentiation. Supporting this, we found significantly elevated levels of OPC differentiation factors IGF-1, BDNF, and Gal-3 in WT mice but not Trem2$^{-/-}$ mice [45, 47]. It is thought that phagocytosis of myelin debris by microglia is crucial for triggering downstream signaling pathways and release of factors that promote OPC differentiation [15, 54]. Thus, the signaling deficit observed in Trem2$^{-/-}$ mice could be due to lack of myelin phagocytosis, which is apparent by the presence of increased debris, and not modulation via TREM2. However, recent work suggests microglia can promote remyelination independent of its role in myelin phagocytosis [2]. Together, our data suggest that TREM2 mediates facets of OPC differentiation and maturation signaling in response to demyelination. Although, the exact mechanism remains unclear, and the set of conditions necessary to induce signaling warrants further investigation.

Oligodendrogenesis is a dynamic, tightly coordinated process principally mediated by interactions with microglia and astrocytes [19, 41, 47]. During remyelination, microglia are preferentially involved in OPC migration, differentiation, and maturation signaling [41, 46, 51]. Interestingly, in WT mice, our data show microglial activation coincided with the initial onset of white matter damage that resolved to a phenotype associated with reparative signaling by 18-months of age. This recapitulates a crucial phenotypic transition from phagocytic 'pro-inflammatory' microglia during migration and proliferation to regenerative 'anti-inflammatory' microglia during differentiation and maturation [15, 41, 46]. TREM2 is known to modulate transition states of microglia into a variety of region- and context-dependent subtypes such as WAMs and DAMs [33, 57]. Accordingly, our data support the idea that this transition from pro-inflammatory to regenerative microglia may be facilitated by TREM2.

Astrocytes have been reported to predominantly support OPC proliferation and mature oligodendrocyte survival [47, 51]. Additionally, microglia can recruit and activate astrocytes through factors like TNF-α, IL-6, and IL-1β that induce a reparative phenotype [11, 29, 34]. Our data show that these signals overlap with an increase in astrocytes in WT mice. In line with this, we saw a positive correlation between the increased presence of

reactive astrocytes and mature oligodendrocyte count. Since we did not observe this in mice lacking TREM2, this implicates TREM2 in modulating the recruitment of reparative astrocytes. Although, given the signaling complexity during remyelination, further validation of these phenotypes and functional outcomes in both microglia and astrocytes is necessary.

Microglial functions influence a host of other extrinsic factors that can also inhibit OPC differentiation, such as myelin debris clearance [9, 35, 36]. Myelin debris clearance is a critical step in remyelination, and inefficient removal can hinder the remyelination process [35, 36]. Additionally, age-related myelin degradation has been shown to have a particular burden on the phagocytic capacity of microglia, causing lysosomal dysfunction and accumulation in the lysosome [42, 56, 60]. Our data show that Trem2$^{-/-}$ mice exhibited significant myelin fragmentation, increased debris volume, and further axonal demyelination with age. There was also lack of activated and CD68^{+} microglia, particularly those elongated and engaged with the white matter tracts (Fig. S3A), that likely promoted and contributed to these outcomes. Furthermore, accumulation of unprocessed myelin debris and lipids was greater in Trem2-deficient microglia than WT microglia (Fig. S3D), which can greatly limit phagocytosis and impact available cholesterol [8, 21, 64].

Cholesterol synthesis in aging white matter is diminished in oligodendrocytes and astrocytes [7, 16]. Therefore, for OPCs to differentiate and remyelinate, exogenous cholesterol in the form of myelin debris must be recycled by microglia [5, 9]. Studies investigating TREM2 loss-of-function mutations or Trem2 deficiency in models of NHD and MS found lysosomal dysfunction and dysregulated lipid metabolism in microglia [21, 48]. Accordingly, in vitro, we found Trem2-deficient microglia displayed reduced myelin uptake coinciding with an inability to upregulate lysosomal genes. Phagocytes overloaded with lipids due to extensive damage or dysfunctional phagocytosis can exhibit ER stress and subsequent UPR activation [21, 24, 28, 48]. Following myelin phagocytosis, we found microglia from both genotypes upregulated UPR genes; although WT microglia upregulated the pro-survival pathway, while Trem2-deficient microglia upregulated the pro-apoptotic pathway. Moreover, reports show TREM2 maintains the metabolic fitness of microglia via mTOR activation and signaling [63]. Impaired mTOR signaling is also associated with increased ER stress-induced apoptosis [21, 28, 63]. Importantly, our data show upregulation of genes associated with the apoptotic UPR pathway still occurred in Trem2-deficient microglia, even at low levels of myelin debris and without apparent phagocytic deficits or overt lipid accumulation. This demonstrates, apart from lipid-induced ER stress, that TREM2 can also modify the ER stress response.

A common response to lipid-induced ER stress is the formation of lipid droplets to maintain homeostasis [21, 48]. Recent publications have identified the emergence of lipid-laden and lipid droplet-accumulating microglia (LDAMs) during aging that are associated with defects in phagocytosis [42, 60]. We found a comparative increase in lipid droplets per cell and denser inclusions indicative of accumulation in Trem2-deficient microglia (Fig. S4C). As LDAMs increase during aging, in conjunction with increasing myelin degeneration, the lipid burden microglia encounter may mediate later dysfunction. Not surprisingly, we found Trem2-deficient microglia confronted with increasing volumes of myelin debris led to a hastened time to phagocytic deficit. Additionally, while Trem2-deficient microglia had no overt issues with lysosomal gene regulation at a comparatively lower volume of myelin debris, defects in uptake still manifested given enough time. These UPR, lysosomal, and lipid droplet differences at low versus high volumes of myelin implies other selective pathways are activated based on severity and duration. This hypothesis is supported by discrepancies reported in lipid droplet accumulation between different contexts (e.g. chronic vs. acute) [9, 21, 24, 48]. Taken together, this suggests that TREM2 beneficially aids microglia from being overwhelmed during age-related degeneration.

Conclusion

We demonstrated Trem2-deficiency aggravates and accelerates age-related myelin degeneration in the striatum. We show this is driven primarily by microglia in two ways: (1) failure to promote conditions permissive to remyelination; and (2) phagocytic deficits in response to demyelination. We identified that TREM2 mediates signaling involved in OPC differentiation/maturation and recruitment of reparative astrocytes. In addition to lysosomal regulation, we show TREM2 can beneficially modulate the ER stress response prior any observable functional microglial deficits or overt pathology. Collectively, as white-matter degeneration progresses with age, the compounding effect of inadequate remyelination conditions in the absence of TREM2 prompts phagocytic deficits that contribute to overwhelming the microglia, further exacerbating pathology. Importantly, our in vitro data revealed there is a debris threshold where Trem2-deficient microglia remain functionally competent for longer durations. As such, targeting/promoting TREM2 function early may augment reparative signaling and prevent overt debris accumulation that leads to premature microglial dysfunction, thus delaying the onset of pathology. Notably, experiments targeting mTOR, the ER, or

cholesterol transporters reduced lipid droplet accumulation and restored functionality in microglia [21, 48]. Our work in conjunction with others shows that modulation of TREM2 function may not only improve phagocytosis, but also augment reparative glial phenotypes and mediate differentiation/maturation signaling to improve remyelination.

Supplementary Information

The online version contains supplementary material available at https://doi.org/10.1186/s40478-024-01855-3.

Supplementary Material 1

Supplementary Material 2

Supplementary Material 3

Supplementary Material 4

Acknowledgements
We would like to thank Guixiang Xu for management of the animal colonies. We would also like to thank Caroline Miller for her advice and input on the electron microscopy. Part of this work was supported by the Center for Electron Microscopy at Indiana University School of Medicine. Figure 4 A was generated using Biorender.com.

Author contributions
Conceptualization: TJM. Methodology and Design: TJM, SJB, and BTL. Experimentation/Data Acquisition: TJM and LMB. Investigation: TJM, LMB, SJB, and BTL. Formal Analysis: TJM. Supervision: SJB and BTL. Manuscript (writing): TJM and SJB. Manuscript (editing): TJM, SJB, LMB, and BTL. All authors read and approved the final manuscript.

Funding
This work was partly supported by the National Institutes of Health (NIH) grant U54 AG054345 (BTL), RF1 AG074566 (BTL, SJB), RF1 AG051495 (BTL) and F31 AG074628 (TJM).

Data availability
The datasets used and/or analyzed during the current study are available from the corresponding author upon request.

Declarations

Ethics approval and consent to participate
The animal experiments were approved by the Institutional Animal Care and Use Committee at Indiana University School of Medicine (protocol #21135) in accordance with all state and federal guidelines.

Consent for publication
Not applicable.

Competing interests
The authors declare that they have no competing interests.

Received: 11 July 2024 / Accepted: 2 August 2024
Published online: 19 September 2024

References

1. Andreone BJ, Przybyla L, Llapashtica C, Rana A, Davis SS, van Lengerich B, Lin K, Shi J, Mei Y, Astarita G al (2020) Alzheimer's-associated PLCgamma2 is a signaling node required for both TREM2 function and the inflammatory response in human microglia. Nat Neurosci 23:927–938. https://doi.org/10.1038/s41593-020-0650-6
2. Baaklini CS, Ho MFS, Lange T, Hammond BP, Panda SP, Zirngibl M, Zia S, Himmelsbach K, Rana H, Phillips Bet al et al (2023) Microglia promote remyelination independent of their role in clearing myelin debris. Cell Rep 42:113574. https://doi.org/10.1016/j.celrep.2023.113574
3. Beckmann N, Neuhaus A, Zurbruegg S, Volkmer P, Patino C, Joller S, Feuerbach D, Doelemeyer A, Schweizer T, Rudin Set al et al (2023) Genetic models of cleavage-reduced and soluble TREM2 reveal distinct effects on myelination and microglia function in the cuprizone model. J Neuroinflammation 20:29. https://doi.org/10.1186/s12974-022-02671-z
4. Bemiller SM, McCray TJ, Allan K, Formica SV, Xu G, Wilson G, Kokiko-Cochran ON, Crish SD, Lasagna-Reeves CA, Ransohoff RM et al (2017) TREM2 deficiency exacerbates tau pathology through dysregulated kinase signaling in a mouse model of tauopathy. Mol Neurodegener 12: 74 https://doi.org/10.1186/s13024-017-0216-6
5. Berghoff SA, Spieth L, Sun T, Hosang L, Schlaphoff L, Depp C, Duking T, Winchenbach J, Neuber J, Ewers Det al et al (2021) Microglia facilitate repair of demyelinated lesions via post-squalene sterol synthesis. Nat Neurosci 24:47–60. https://doi.org/10.1038/s41593-020-00757-6
6. Boggs JM (2006) Myelin basic protein: a multifunctional protein. Cell Mol Life Sci 63:1945–1961. https://doi.org/10.1007/s00018-006-6094-7
7. Boisvert MM, Erikson GA, Shokhirev MN, Allen NJ (2018) The aging astrocyte transcriptome from multiple regions of the mouse brain. Cell Rep 22:269–285. https://doi.org/10.1016/j.celrep.2017.12.039
8. Cantoni C, Bollman B, Licastro D, Xie M, Mikesell R, Schmidt R, Yuede CM, Galimberti D, Olivecrona G, Klein RS et al (2015) TREM2 regulates microglial cell activation in response to demyelination in vivo. Acta Neuropathol 129: 429–447 https://doi.org/10.1007/s00401-015-1388-1
9. Cantuti-Castelvetri L, Fitzner D, Bosch-Queralt M, Weil MT, Su M, Sen P, Ruhwedel T, Mitkovski M, Trendelenburg G, Lutjohann D et al (2018) Defective cholesterol clearance limits remyelination in the aged central nervous system. Science 359: 684–688 https://doi.org/10.1126/science.aan4183
10. Cignarella F, Filipello F, Bollman B, Cantoni C, Locca A, Mikesell R, Manis M, Ibrahim A, Deng L, Benitez BA al (2020) TREM2 activation on microglia promotes myelin debris clearance and remyelination in a model of multiple sclerosis. Acta Neuropathol 140:513–534. https://doi.org/10.1007/s00401-020-02193-z
11. Clarke LE, Liddelow SA, Chakraborty C, Munch AE, Heiman M, Barres BA (2018) Normal aging induces A1-like astrocyte reactivity. Proc Natl Acad Sci U S A 115: E1896-E1905 https://doi.org/10.1073/pnas.1800165115
12. Coelho A, Fernandes HM, Magalhaes R, Moreira PS, Marques P, Soares JM, Amorim L, Portugal-Nunes C, Castanho T, Santos NC al (2021) Signatures of white-matter microstructure degradation during aging and its association with cognitive status. Sci Rep 11:4517. https://doi.org/10.1038/s41598-021-83983-7
13. Cox SR, Ritchie SJ, Tucker-Drob EM, Liewald DC, Hagenaars SP, Davies G, Wardlaw JM, Gale CR, Bastin ME, Deary IJ (2016) Ageing and brain white matter structure in 3,513 UK Biobank participants. Nat Commun 7:13629. https://doi.org/10.1038/ncomms13629
14. Crawford AH, Tripathi RB, Richardson WD, Franklin RJM (2016) Developmental Origin of Oligodendrocyte Lineage cells determines response to demyelination and susceptibility to Age-Associated Functional decline. Cell Rep 15:761–773. https://doi.org/10.1016/j.celrep.2016.03.069
15. Cunha MI, Su M, Cantuti-Castelvetri L, Muller SA, Schifferer M, Djannatian M, Alexopoulos I, van der Meer F, Winkler A, van Ham TJ et al (2020) Pro-inflammatory activation following demyelination is required for myelin clearance and oligodendrogenesis. J Exp Med 217: https://doi.org/10.1084/jem.20191390
16. de la Fuente AG, Queiroz RML, Ghosh T, McMurran CE, Cubillos JF, Bergles DE, Fitzgerald DC, Jones CA, Lilley KS, Glover CPet al et al (2020) Changes in the Oligodendrocyte Progenitor Cell Proteome with Ageing. Mol Cell Proteom 19:1281–1302. https://doi.org/10.1074/mcp.RA120.002102
17. Depp C, Sun T, Sasmita AO, Spieth L, Berghoff SA, Nazarenko T, Overhoff K, Steixner-Kumar AA, Subramanian S, Arinrad Set al et al (2023) Myelin dysfunction drives amyloid-beta deposition in models of Alzheimer's disease. Nature 618:349–357. https://doi.org/10.1038/s41586-023-06120-6
18. Desai MK, Mastrangelo MA, Ryan DA, Sudol KL, Narrow WC, Bowers WJ (2010) Early oligodendrocyte/myelin pathology in Alzheimer's disease mice constitutes a novel therapeutic target. Am J Pathol 177:1422–1435. https://doi.org/10.2353/ajpath.2010.100087
19. Domingues HS, Portugal CC, Socodato R, Relvas JB (2016) Oligodendrocyte, astrocyte, and Microglia Crosstalk in Myelin Development, damage, and repair. Front Cell Dev Biol 4:71. https://doi.org/10.3389/fcell.2016.00071

20. Duncan ID, Marik RL, Broman AT, Heidari M (2017) Thin myelin sheaths as the hallmark of remyelination persist over time and preserve axon function. Proc Natl Acad Sci U S A 114:E9685–E9691. https://doi.org/10.1073/pnas.1714183114
21. Filipello F, You SF, Mirfakhar FS, Mahali S, Bollman B, Acquarone M, Korvatska O, Marsh JA, Sivaraman A, Martinez R al (2023) Defects in lysosomal function and lipid metabolism in human microglia harboring a TREM2 loss of function mutation. Acta Neuropathol 145:749–772. https://doi.org/10.1007/s00401-023-02568-y
22. Forabosco P, Ramasamy A, Trabzuni D, Walker R, Smith C, Bras J, Levine AP, Hardy J, Pocock JM, Guerreiro Ret al et al (2013) Insights into TREM2 biology by network analysis of human brain gene expression data. Neurobiol Aging 34:2699–2714. https://doi.org/10.1016/j.neurobiolaging.2013.05.001
23. Franklin RJM, Ffrench-Constant C (2017) Regenerating CNS myelin - from mechanisms to experimental medicines. Nat Rev Neurosci 18:753–769. https://doi.org/10.1038/nrn.2017.136
24. Gouna G, Klose C, Bosch-Queralt M, Liu L, Gokce O, Schifferer M, Cantuti-Castelvetri L, Simons M (2021) TREM2-dependent lipid droplet biogenesis in phagocytes is required for remyelination. J Exp Med 218. https://doi.org/10.1084/jem.20210227
25. Grabert K, Michoel T, Karavolos MH, Clohisey S, Baillie JK, Stevens MP, Freeman TC, Summers KM, McColl BW (2016) Microglial brain region-dependent diversity and selective regional sensitivities to aging. Nat Neurosci 19:504–516. https://doi.org/10.1038/nn.4222
26. Hahn O, Foltz AG, Atkins M, Kedir B, Moran-Losada P, Guldner IH, Munson C, Kern F, Palovics R, Lu N (2023) al Atlas of the aging mouse brain reveals white matter as vulnerable foci. Cell 186: 4117–4133 e4122 https://doi.org/10.1016/j.cell.2023.07.027
27. Harauz G, Boggs JM (2013) Myelin management by the 18.5-kDa and 21.5-kDa classic myelin basic protein isoforms. J Neurochem 125:334–361. https://doi.org/10.1111/jnc.12195
28. Hetz C, Zhang K, Kaufman RJ (2020) Mechanisms, regulation and functions of the unfolded protein response. Nat Rev Mol Cell Biol 21:421–438. https://doi.org/10.1038/s41580-020-0250-z
29. Hyvarinen T, Hagman S, Ristola M, Sukki L, Veijula K, Kreutzer J, Kallio P, Narkilahti S (2019) Co-stimulation with IL-1beta and TNF-alpha induces an inflammatory reactive astrocyte phenotype with neurosupportive characteristics in a human pluripotent stem cell model system. Sci Rep 9:16944. https://doi.org/10.1038/s41598-019-53414-9
30. Itoh N, Itoh Y, Tassoni A, Ren E, Kaito M, Ohno A, Ao Y, Farkhondeh V, Johnsonbaugh H, Burda J al (2018) Cell-specific and region-specific transcriptomics in the multiple sclerosis model: focus on astrocytes. Proc Natl Acad Sci U S A 115:E302–E309. https://doi.org/10.1073/pnas.1716032115
31. Jay TR, Hirsch AM, Broihier ML, Miller CM, Neilson LE, Ransohoff RM, Lamb BT, Landreth GE (2017) Disease Progression-Dependent effects of TREM2 Deficiency in a mouse model of Alzheimer's Disease. J Neurosci 37:637–647. https://doi.org/10.1523/JNEUROSCI.2110-16.2016
32. Kaiser T, Allen HM, Kwon O, Barak B, Wang J, He Z, Jiang M, Feng G (2021) MyelTracer: A Semi-automated Software for myelin g-Ratio quantification. eNeuro 8. https://doi.org/10.1523/ENEURO.0558-20.2021
33. Keren-Shaul H, Spinrad A, Weiner A, Matcovitch-Natan O, Dvir-Szternfeld R, Ulland TK, David E, Baruch K, Lara-Astaiso D, Toth B et al (2017) A Unique Microglia Type Associated with Restricting Development of Alzheimer's Disease. Cell 169: 1276–1290 e1217 https://doi.org/10.1016/j.cell.2017.05.018
34. Kiray H, Lindsay SL, Hosseinzadeh S, Barnett SC (2016) The multifaceted role of astrocytes in regulating myelination. Exp Neurol 283:541–549. https://doi.org/10.1016/j.expneurol.2016.03.009
35. Kotter MR, Li WW, Zhao C, Franklin RJ (2006) Myelin impairs CNS remyelination by inhibiting oligodendrocyte precursor cell differentiation. J Neurosci 26:328–332. https://doi.org/10.1523/JNEUROSCI.2615-05.2006
36. Lampron A, Larochelle A, Laflamme N, Prefontaine P, Plante MM, Sanchez MG, Yong VW, Stys PK, Tremblay ME, Rivest S (2015) Inefficient clearance of myelin debris by microglia impairs remyelinating processes. J Exp Med 212:481–495. https://doi.org/10.1084/jem.20141656
37. Lattante S, Le Ber I, Camuzat A, Dayan S, Godard C, Van Bortel I, De Septenville A, Ciura S, Brice A, Kabashi Eet al et al (2013) TREM2 mutations are rare in a French cohort of patients with frontotemporal dementia. Neurobiol Aging 34:2443e2441–2443e2442. https://doi.org/10.1016/j.neurobiolaging.2013.04.030
38. Lee S, Viqar F, Zimmerman ME, Narkhede A, Tosto G, Benzinger TL, Marcus DS, Fagan AM, Goate A, Fox NCet al et al (2016) White matter hyperintensities are a core feature of Alzheimer's disease: evidence from the dominantly inherited Alzheimer network. Ann Neurol 79:929–939. https://doi.org/10.1002/ana.24647
39. Leyns CEG, Ulrich JD, Finn MB, Stewart FR, Koscal LJ, Remolina Serrano J, Robinson GO, Anderson E, Colonna M, Holtzman DM (2017) TREM2 deficiency attenuates neuroinflammation and protects against neurodegeneration in a mouse model of tauopathy. Proc Natl Acad Sci U S A 114:11524–11529. https://doi.org/10.1073/pnas.1710311114
40. Linnartz-Gerlach B, Bodea LG, Klaus C, Ginolhac A, Halder R, Sinkkonen L, Walter J, Colonna M, Neumann H (2019) TREM2 triggers microglial density and age-related neuronal loss. Glia 67:539–550. https://doi.org/10.1002/glia.23563
41. Lloyd AF, Miron VE (2019) The pro-remyelination properties of microglia in the central nervous system. Nat Rev Neurol 15:447–458. https://doi.org/10.1038/s41582-019-0184-2
42. Marschallinger J, Iram T, Zardeneta M, Lee SE, Lehallier B, Haney MS, Pluvinage JV, Mathur V, Hahn O, Morgens DW al (2020) Lipid-droplet-accumulating microglia represent a dysfunctional and proinflammatory state in the aging brain. Nat Neurosci 23:194–208. https://doi.org/10.1038/s41593-019-0566-1
43. McKenzie AT, Moyon S, Wang M, Katsyv I, Song WM, Zhou X, Dammer EB, Duong DM, Aaker J, Zhao Y al (2017) Multiscale network modeling of oligodendrocytes reveals molecular components of myelin dysregulation in Alzheimer's disease. Mol Neurodegener 12:82. https://doi.org/10.1186/s13024-017-0219-3
44. McNamara NB, Munro DAD, Bestard-Cuche N, Uyeda A, Bogie JFJ, Hoffmann A, Holloway RK, Molina-Gonzalez I, Askew KE, Mitchell Set al et al (2023) Microglia regulate central nervous system myelin growth and integrity. Nature 613:120–129. https://doi.org/10.1038/s41586-022-05534-y
45. Miron VE (2017) Microglia-driven regulation of oligodendrocyte lineage cells, myelination, and remyelination. J Leukoc Biol 101:1103–1108. https://doi.org/10.1189/jlb.3RI1116-494R
46. Miron VE, Boyd A, Zhao JW, Yuen TJ, Ruckh JM, Shadrach JL, van Wijngaarden P, Wagers AJ, Williams A, Franklin RJM al (2013) M2 microglia and macrophages drive oligodendrocyte differentiation during CNS remyelination. Nat Neurosci 16:1211–1218. https://doi.org/10.1038/nn.3469
47. Molina-Gonzalez I, Holloway RK, Jiwaji Z, Dando O, Kent SA, Emelianova K, Lloyd AF, Forbes LH, Mahmood A, Skripuletz T et al (2023) Astrocyte-oligodendrocyte interaction regulates central nervous system regeneration. Nat Commun 14: 3372 https://doi.org/10.1038/s41467-023-39046-8
48. Nugent AA, Lin K, van Lengerich B, Lianoglou S, Przybyla L, Davis SS, Llapashtica C, Wang J, Kim DJ, Xia Det al et al (2020) TREM2 Regulates Microglial Cholesterol Metabolism upon Chronic Phagocytic Challenge. Neuron 105: 837–854 e839 https://doi.org/10.1016/j.neuron.2019.12.007
49. Oost W, Huitema AJ, Kats K, Giepmans BNG, Kooistra SM, Eggen BJL, Baron W (2023) Pathological ultrastructural alterations of myelinated axons in normal appearing white matter in progressive multiple sclerosis. Acta Neuropathol Commun 11:100. https://doi.org/10.1186/s40478-023-01598-7
50. Paloneva J, Manninen T, Christman G, Hovanes K, Mandelin J, Adolfsson R, Bianchin M, Bird T, Miranda R, Salmaggi A al (2002) Mutations in two genes encoding different subunits of a receptor signaling complex result in an identical disease phenotype. Am J Hum Genet 71:656–662. https://doi.org/10.1086/342259
51. Pang Y, Fan LW, Tien LT, Dai X, Zheng B, Cai Z, Lin RC, Bhatt A (2013) Differential roles of astrocyte and microglia in supporting oligodendrocyte development and myelination in vitro. Brain Behav 3:503–514. https://doi.org/10.1002/brb3.152
52. Poliani PL, Wang Y, Fontana E, Robinette ML, Yamanishi Y, Gilfillan S, Colonna M (2015) TREM2 sustains microglial expansion during aging and response to demyelination. J Clin Invest 125:2161–2170. https://doi.org/10.1172/JCI77983
53. Powers BE, Sellers DL, Lovelett EA, Cheung W, Aalami SP, Zapertov N, Maris DO, Horner PJ (2013) Remyelination reporter reveals prolonged refinement of spontaneously regenerated myelin. Proc Natl Acad Sci U S A 110:4075–4080. https://doi.org/10.1073/pnas.1210293110
54. Qin C, Yang S, Chen M, Dong MH, Zhou LQ, Chu YH, Shen ZX, Bosco DB, Wu LJ, Tian DS al (2023) Modulation of microglial metabolism facilitates regeneration in demyelination. iScience 26:106588. https://doi.org/10.1016/j.isci.2023.106588
55. Rawji KS, Neumann B, Franklin RJM (2023) Glial aging and its impact on central nervous system myelin regeneration. Ann N Y Acad Sci 1519:34–45. https://doi.org/10.1111/nyas.14933
56. Safaiyan S, Kannaiyan N, Snaidero N, Brioschi S, Biber K, Yona S, Edinger AL, Jung S, Rossner MJ, Simons M (2016) Age-related myelin degradation

burdens the clearance function of microglia during aging. Nat Neurosci 19:995–998. https://doi.org/10.1038/nn.4325
57. Safaiyan S, Besson-Girard S, Kaya T, Cantuti-Castelvetri L, Liu L, Ji H, Schifferer M, Gouna G, Usifo F, Kannaiyan Net al et al (2021) White matter aging drives microglial diversity. Neuron 109: 1100–1117 e1110 https://doi.org/10.1016/j.neuron.2021.01.027
58. Saggu SK, Chotaliya HP, Blumbergs PC, Casson RJ (2010) Wallerian-like axonal degeneration in the optic nerve after excitotoxic retinal insult: an ultrastructural study. BMC Neurosci 11:97. https://doi.org/10.1186/1471-2202-11-97
59. Sharaf A, Krieglstein K, Spittau B (2013) Distribution of microglia in the postnatal murine nigrostriatal system. Cell Tissue Res 351:373–382. https://doi.org/10.1007/s00441-012-1537-y
60. Shimabukuro MK, Langhi LG, Cordeiro I, Brito JM, Batista CM, Mattson MP, Mello Coelho V (2016) Lipid-laden cells differentially distributed in the aging brain are functionally active and correspond to distinct phenotypes. Sci Rep 6:23795. https://doi.org/10.1038/srep23795
61. Sim FJ, Zhao C, Penderis J, Franklin RJ (2002) The age-related decrease in CNS remyelination efficiency is attributable to an impairment of both oligodendrocyte progenitor recruitment and differentiation. J Neurosci 22:2451–2459. https://doi.org/10.1523/JNEUROSCI.22-07-02451.2002
62. Takahashi K, Prinz M, Stagi M, Chechneva O, Neumann H (2007) TREM2-transduced myeloid precursors mediate nervous tissue debris clearance and facilitate recovery in an animal model of multiple sclerosis. PLoS Med 4:e124. https://doi.org/10.1371/journal.pmed.0040124
63. Ulland TK, Song WM, Huang SC, Ulrich JD, Sergushichev A, Beatty WL, Loboda AA, Zhou Y, Cairns NJ, Kambal Aet al et al (2017) TREM2 Maintains Microglial Metabolic Fitness in Alzheimer's Disease. Cell 170: 649–663 e613 https://doi.org/10.1016/j.cell.2017.07.023
64. Wang Y, Cella M, Mallinson K, Ulrich JD, Young KL, Robinette ML, Gilfillan S, Krishnan GM, Sudhakar S, Zinselmeyer BHet al et al (2015) TREM2 lipid sensing sustains the microglial response in an Alzheimer's disease model. Cell 160:1061–1071. https://doi.org/10.1016/j.cell.2015.01.049
65. Wang Y, Kyauk RV, Shen YA, Xie L, Reichelt M, Lin H, Jiang Z, Ngu H, Shen K, Greene JJ al (2023) TREM2-dependent microglial function is essential for remyelination and subsequent neuroprotection. Glia 71:1247–1258. https://doi.org/10.1002/glia.24335
66. Weil MT, Mobius W, Winkler A, Ruhwedel T, Wrzos C, Romanelli E, Bennett JL, Enz L, Goebels N, Nave KA al (2016) Loss of myelin basic protein function triggers myelin breakdown in models of demyelinating diseases. Cell Rep 16:314–322. https://doi.org/10.1016/j.celrep.2016.06.008
67. Westlye LT, Walhovd KB, Dale AM, Bjornerud A, Due-Tonnessen P, Engvig A, Grydeland H, Tamnes CK, Ostby Y, Fjell AM (2010) Life-span changes of the human brain white matter: diffusion tensor imaging (DTI) and volumetry. Cereb Cortex 20:2055–2068. https://doi.org/10.1093/cercor/bhp280
68. Wingo AP, Fan W, Duong DM, Gerasimov ES, Dammer EB, Liu Y, Harerimana NV, White B, Thambisetty M, Troncoso JC al (2020) Shared proteomic effects of cerebral atherosclerosis and Alzheimer's disease on the human brain. Nat Neurosci 23:696–700. https://doi.org/10.1038/s41593-020-0635-5
69. Ximerakis M, Lipnick SL, Innes BT, Simmons SK, Adiconis X, Dionne D, Mayweather BA, Nguyen L, Niziolek Z, Ozek Cet al et al (2019) Single-cell transcriptomic profiling of the aging mouse brain. Nat Neurosci 22:1696–1708. https://doi.org/10.1038/s41593-019-0491-3
70. You YF, Chen M, Tang Y, Yu WX, Pang XW, Chu YH, Zhang H, Shang K, Deng G, Zhou LQ (2023) al TREM2 deficiency inhibits microglial activation and aggravates demyelinating injury in neuromyelitis optica spectrum disorder. J Neuroinflammation 20: 89 https://doi.org/10.1186/s12974-023-02772-3

Publisher's note

Springer Nature remains neutral with regard to jurisdictional claims in published maps and institutional affiliations.